Weldability of Aluminum Alloys with High-Power Diode Laser

Higher penetration than previously reported under the conduction regime were obtained in welds of six aluminum alloys

BY J. M. SÁNCHEZ-AMAYA, Z. BOUKHA, M. R. AMAYA-VÁZQUEZ, AND F. J. BOTANA.

ABSTRACT

In the present work, a high-power diode laser has been employed to weld six aluminum alloys (1050, 2017, 2024, 5083, 6082, and 7075) under conduction regime. Controlling the experimental variables, butt joints with higher penetration than those previously reported in the literature for this regime could be obtained, demonstrating the weldability of all these alloys with the employed methodology. Afterward, the depths and widths of the beads were fitted to a simple mathematical equation proposed by the authors. Taking into account the weld penetration values and the susceptibility to solidification cracking, the weldability order was seen to be: 5083 > 7075 > 2017 = 2024 = 6082 > 1050. The magnesium content and, to a lower extent, the zinc and silicon amount were observed to improve the weldability of the aluminum alloys.

Introduction

Laser beam welding (LBW) is becoming an important industrial technology, being used in a great variety of processes due to its low heat input, high welding speed, high flexibility, high weld quality, and high production rate (Refs. 1–5). LBW is also reported elsewhere (Refs. 1, 5–8) to be difficult to implement to aluminum alloys because of their high reflectivity (leading to absorption of a small fraction of the incident radiation), high thermal conductivity (provoking a fast heat transfer in the welding piece that limits the concentration of energy in the weld pool), and low viscosity (restricting the growth of the weld pool before solidification).

Two laser welding regimes are reported in the literature (Refs. 2, 9, 10), so-called keyhole (or deep penetration) and conduction (limited to conduction). The former mode requires the application of higher power densities (typically above 10^6 W/cm^2) than the latter (below 10^6 W/cm^2). Under the keyhole regime, the high input energy allows the obtaining of deep-penetration joints, although it provokes high metal evaporation. In contrast, the conduction regime is a more stable process, as metal vaporization is diminished due to the lower input laser energy (Refs. 2, 10). Although the conduction regime usually generates limited penetration welds, its stability improves the weld quality, offering an alternative joining mode for difficult-to-weld materials such as aluminum alloys.

Numerous studies dealing with laser welding of aluminum alloys are presently available (Refs. 4, 11–18), though few of them were performed under the conduction regime (Refs. 1, 2, 8, 11, 19). High-power CO_2 (Refs. 13–16) and Nd:YAG (Refs. 4, 11, 12, 18) lasers were the most used equipment for these applications. High-power laser diode (HPDL) was employed in relatively few works (Refs. 1, 2, 19), although it offers a clear advantage: The absorption of the HPDL wavelength by aluminum alloys is higher than the CO_2 and Nd:YAG wavelengths (Ref. 20). Thus, the emission wavelength of the HPDL (808 nm) provokes a higher absorptivity in aluminum than the longer wavelengths of Nd:YAG (1064 nm) and CO_2 (10640 nm) lasers.

In the literature, rather low values of weld penetration have been obtained in aluminum alloys under the conduction regime. Thus, complete penetration (1 mm) bead-on-plate and butt-joint welds of 5XXX and 6XXX aluminum alloys are obtained with a HPDL (Ref. 19). Bead-on-plate conduction welds of 5182 aluminum alloy of 1 mm thickness were also obtained in Ref. 11 using a Nd:YAG laser. More recently, higher penetration conduction butt joints have been reported by the authors (Ref. 1), reaching penetration values up to 3.0 mm in Alloy 5083 and 2.3 mm in Alloy 6082.

The great majority of the studies dealing with laser welding of aluminum alloys under the conduction regime are devoted to investigating the influence of laser process conditions on the weld properties. However, much less numerous are papers focused on the study of the weld geometry (Refs. 1, 8, 11). Thus, a model has been developed to study the evaporation rate, fusion zone geometry, and the compositional changes in 5182 aluminum alloy, showing a reasonable agreement with the experimental results (Ref. 11). Additionally, a three-dimensional numerical model has been developed in Ref. 8 to analyze laser welding of 5083 aluminum alloy, allowing the authors to obtain the morphology, velocity field, and temperature field of the melted zone in steady state. The predicted dimensions of the weld pool agreed well with experimental results (Ref. 8). A morphological study of 5083 and 6082 butt joints was performed in Ref. 1. The obtained depth values were fitted to an equation that allows the estimation of weld penetration from the input values of laser power and welding speed.

The first objective of the present work has been to study the possibility of obtaining high-penetration welds of six aluminum alloys (1050, 2017, 2024, 5083, 6082, and 7075) with a HPDL under the conduction regime. Although high welding depths have been previously reported in 5083 and 6082 samples (Ref. 1), the applicability of HPDL to obtain high-penetration welds in other aluminum alloys has

KEYWORDS

Laser Beam Welding
Conduction Regime
Aluminum Alloys 1050, 2017, 2024, 5083, 6082, 7075
Experimental Fitting
High-Power Diode Laser

J. M. SÁNCHEZ-AMAYA (josemaria.sanchez@titania.aero) *is with Titania, Tests and Industrial Projects, S.L. (Titania, Ensayos y Proyectos Industriales S.L.), Cádiz, Spain. Z. BOUKHA, M. R. AMAYA-VÁZQUEZ, and F. J. BOTANA are with LABCYP, Department of Materials Science, Metallurgy, and Inorganic Chemistry (Departamento de Ciencia de los Materiales e Ingeniería Metalúrgica y Química Inorgánica), University of Cádiz, Cádiz, Spain.*

Fig. 1 — Laser equipment and mobile X-Y table.

not yet been studied. The second objective has been to analyze the fitting degree of a simple mathematical expression proposed by the authors to the experimental weld depths obtained for the six aluminum alloys. The last aim has been to compare the weldability of the six aluminum alloys, taking into account the alloying elements.

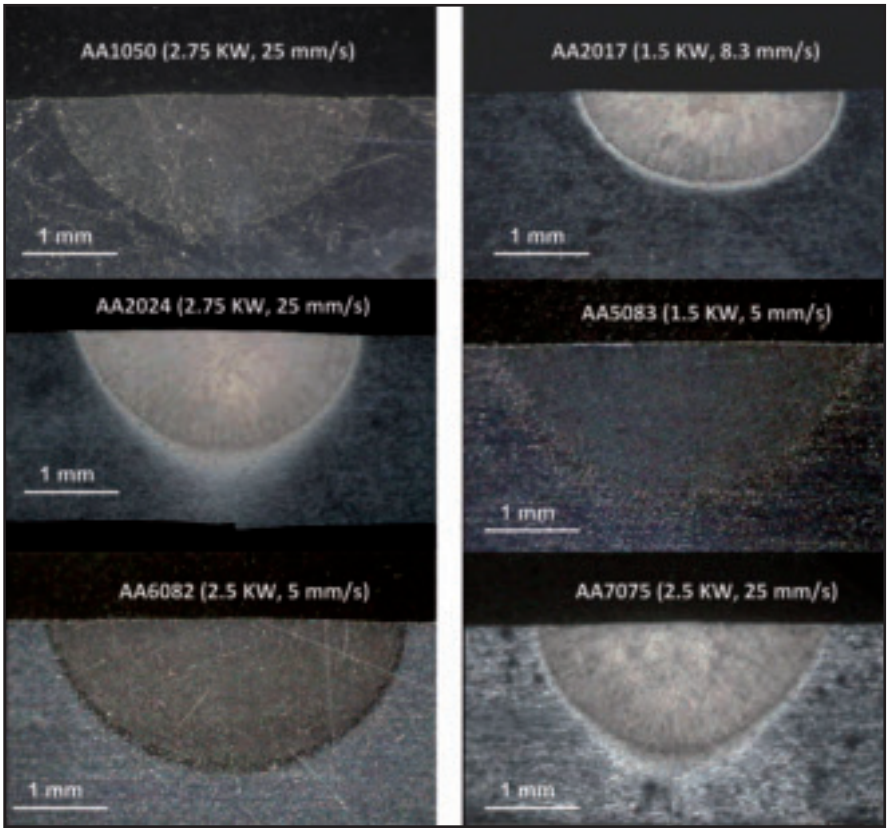

Fig. 2 — Examples of metallographic images (30×) of butt-joint weld beads in aluminum alloys, obtained with the indicated laser power and welding rate conditions.

Table 1 — Chemical Compositions of Aluminum Alloys (wt-%)

Element	Si	Fe	Cu	Mn	Mg	Zn	Cr	Ti	Ga	V	Al
1050-T0	0.13	0.32	<0.01	<0.01	<0.01	0.02	<0.01	<0.01	<0.01	<0.01	99.50
2017-T3	0.62	0.51	3.83	0.59	0.53	0.10	0.01	0.03	<0.01	<0.01	93.70
2024-T3	0.10	0.22	4.11	0.56	1.34	0.13	0.01	0.01	0.01	<0.01	93.49
5083-T0	0.10	0.30	0.02	0.50	4.22	<0.01	0.08	0.02	0.01	0.01	94.73
6082-T6	1.03	0.34	0.06	0.57	0.87	0.01	0.01	0.03	0.01	<0.01	97.04
7075-T6	0.06	0.16	1.25	0.08	2.32	5.47	0.20	0.01	0.01	0.01	90.41

Material and Methods

Six aluminum alloys (1050, 2017, 2024, 5083, 6082, and 7075) were welded under the conduction regime by means of a high-power diode laser. The size of the processed samples was 70 mm long and 14 mm wide. In a first part of the study in which the influence of the experimental variables were analyzed, butt joints were generated on samples with the thickness in which the sheet alloys were provided: 2 mm (1050, 2024, and 7075), 3 mm (5083), and 4 mm (2017 and 6082). In a second analysis in which the weldability of the different alloys was compared, bead-on-plate welds were generated on samples of 70 × 14 × 2 mm^3, the thickness of 5083, 2017, and 6082 plates having been reduced to 2 mm. The compositions of these alloys are included in Table 1. All samples were sandblasted with corindon particles to promote laser absorption (Refs. 1, 2). According to recent measurements performed in our laboratory, this superficial treatment lead to absorptivity values around 50% in 5083 samples. In addition to improving the laser absorption, the application of sandblasting as previous superficial treatments leads to low magnesium evaporation in the welds obtained under the conduction regime (Ref. 2). Thus, while other superficial treatments, such as the application of dark coatings, generate weld beads with magnesium lost up to 4%, sandblasting limits this evaporation up to 1%, leading consequently to improvements on the corrosion behavior

Table 2 — Laser Power (*P*) and Welding Speed (*v*) Conditions to Obtain Butt Joints on Aluminum Alloy Samples

Aluminum Alloys	*P*/kW	*v*/mm·s^{-1}
1050	1.5, 2, 2.5, and 2.75	(5), 8.3, 13.3, 16.6, 25
2017	1.5, 2, 2.5, and 2.75	5, 8.3, 16.6, 25
2024	1.5, 2, 2.5, and 2.75	(5), (8.3), 13.3, 16.6, 25
5083	1.5, 2, 2.5, and 2.75	5, 8.3, 16.6, 25, 50, 75, 100
6082	2, 2.5, and 2.75	3.3, 5, 8.3, 16.6, (50), (83)
7075	1.5, 2, 2.5, and 2.75	(8.3), 16.6, 25, 33.3

Table 3 — Width (*w*) and Depth (*d*) Values of Butt Joints of the Six Aluminum Alloys, in Function of the Laser Power (*P*) and the Welding Speed (*v*)

AA1050

P (kW)	*v* (mm/s)	d/w
1.5	5.00	2.00/4.98
1.5	8.33	1.36/3.19
1.5	13.33	0.99/2.83
1.5	16.67	0.73/2.52
2	8.33	1.71/3.65
2	13.33	1.02/2.84
2	16.67	0.99/2.90
2	25.00	0.99/2.86
2.5	8.33	2.00/3.69
2.5	13.33	1.30/3.26
2.5	16.67	1.20/3.12
2.5	25.00	1.05/2.86
2.75	13.33	1.31/3.52
2.75	16.67	1.23/3.21
2.75	25.00	1.12/2.90

AA2017

P (kW)	*v* (mm/s)	d/w
1.5	5.00	1.33/3.69
1.5	8.33	1.13/3.14
1.5	16.67	0.82/2.66
2	5.00	1.49/4.18
2	8.33	1.22/3.47
2	16.67	0.95/2.97
2.5	5.00	1.70/4.50
2.5	8.33	1.32/3.84
2.5	16.67	1.05/3.07
2.5	25.00	0.87/2.98
2.75	5.00	1.72/4.70
2.75	8.33	1.30/3.85
2.75	16.67	1.11/3.33
2.75	25.00	0.97/3.11

AA2024

P (kW)	*v* (mm/s)	d/w
1.5	5.00	2.00/4.76
1.5	8.33	1.99/3.62
1.5	13.33	1.31/3.01
1.5	16.67	1.25/2.93
2.0	5.00	2.00/5.70
2.0	8.33	2.00/4.11
2.0	13.33	1.68/3.46
2.0	16.67	1.40/3.23
2.0	25.00	1.32/2.89
2.5	5.00	2.00/6.46
2.5	8.33	2.00/4.42
2.5	13.33	2.00/3.75
2.5	16.67	1.53/3.50
2.5	25.00	1.46/3.11
2.75	5.00	2.00/6.52
2.75	8.33	2.00/4.63
2.75	13.33	2.00/3.95
2.75	16.67	1.59/3.58
2.75	25.00	1.34/3.13

AA5083

P (kW)	*v* (mm/s)	d/w
1.5	5.00	1.93/4.09
1.5	8.33	1.36/3.66
1.5	16.67	1.10/2.94
1.5	25.00	0.91/2.65
1.5	50.00	0.71/2.31
2	5.00	2.38/4.67
2	8.33	1.62/3.92
2	16.67	1.16/3.18
2	25.00	1.00/2.88
2	50	0.73/2.52
2	75	0.72/2.34
2	100	0.80/2.34
2.5	5	2.72/5.34
2.5	8.33	1.85/4.41
2.5	16.67	1.20/3.42
2.5	25	1.09/3.11
2.5	50	0.79/2.67
2.5	75	0.70/2.49
2.5	100	0.84/2.48
2.75	5	3.00/5.90
2.75	8.33	2.08/4.70
2.75	16.67	1.29/3.60
2.75	25	1.13/3.25
2.75	50	0.84/2.76
2.75	75	0.87/2.60
2.75	100	0.94/2.58

AA6082

P (kW)	*v* (mm/s)	d/w
2	3.33	1.85/4.09
2	5	1.20/3.21
2	8.33	1.11/2.99
2	16.67	0.83/2.52
2	50	0.70/2.26
2	83.35	0.54/1.94
2.5	3.33	2.11/4.67
2.5	5	1.45/3.82
2.5	8.33	1.20/3.31
2.5	16.67	0.91/2.88
2.5	50	0.72/2.39
2.5	83.35	0.56/2.11
2.75	3.33	2.29/5.07
2.75	5	1.54/3.89
2.75	8.33	1.20/3.39
2.75	16.67	0.96/2.92
2.75	50	0.83/2.56
2.75	83.35	0.70/2.12

AA7075

P (kW)	*v* (mm/s)	d/w
1.5	8.33	2/4.41
1.5	16.67	1.45/3.32
1.5	25	1.15/2.90
2	8.33	2.00/5.00
2	16.67	1.66/3.65
2	25	1.21/3.13
2	33.33	1.09/2.94
2.5	8.33	2.00/5.35
2.5	16.67	2.00/4.18
2.5	25	1.43/3.38
2.5	33.33	1.21/3.1
2.75	8.33	2.00/5.40
2.75	16.67	2.00/4.27
2.75	25	1.46/3.52
2.75	33.33	1.18/3.19

of the melted zone (Ref. 2).

A high-power diode laser, Rofin Model DL028S, with a maximum power of 2.8 kW, was employed to weld the aluminum alloy samples. Figure 1 includes an image of the laser equipment and the mobile X-Y table, whose movement was controlled by *Visual Setup* software. The laser beam conditions were the same as reported in Ref. 1. Thus, the surface samples were kept at the focal position (spot size on surface is 2.2 × 1.7 mm), working the laser source in continuous mode. The laser treatment always consisted of one single linear scan of 60 mm, performed at the interface between the pair of samples to be welded (in butt joining) or at the center of a single sample (in bead-on-plate welding). In order to concentrate the laser energy, the welding direction was the X axis, the configuration providing a lower width (1.7 mm) of the linear laser source. Nitrogen was always employed as the shielding gas, at a flow rate of 15 NL/min, avoiding the oxide formation in aluminum alloy welds (Refs. 5, 7). Although argon is more commonly used as the shielding gas for LBW of aluminum alloys (because it minimizes the formation of gas porosity), nitrogen has been employed in this research because it was considered interesting to test a cheaper shielding gas, taking into account that LBW was performed under conduction mode. This regime leads to highly stable weld pools, and therefore produces welds with lower porosity than those generated under keyhole regime (Ref. 1).

The laser power *(P)* and welding speed *(v)* employed to obtain the butt joints of each alloy are detailed in Table 2. As can be seen, *P* ranged between 1.5 and 2.75 kW and *v* between 0.2 and 6 m/min (3.3 and 100 mm/s), the low and upper limits of both variables having been determined experimentally. Thus, the fluences of these laser treatments ranged between 0.9 kJ·cm^{-2} (for P = 2 kW and v = 100 mm/s) and 37.5 kJ·cm^{-2} (for P = 2.75 kW and v = 3.3 mm/s). The inferior limits (the less energetic condition, with low *P* and high *v*) of each alloy were those leading to weak welds. Lower aggressive conditions than this lower limit were discarded, as the input energy was not high enough to generate and stabilize a weld pool leading to the joint. On the other hand, the upper limits (high *P* and low *v*) were those provoking complete-joint-penetration welds. The welding speed values leading to both lowest and highest energetic conditions have been marked between brackets in Table 2.

The bead-on-plate laser treatments were performed at two rates: 16.6 and 33.3 mm/s, keeping invariable the rest of the experimental conditions (sandblasted samples, P = 2 kW, 15 L/min N_2, etc.). These treatments correspond to laser fluences of 5.5 and 2.7 kJ·cm^{-2}, respectively.

The depth and width of butt-joint and

bead-on-plate welds were measured from metallographic images of the bead cross-sections, after cutting, mounting, polishing, and etching (with Keller) the welds. Each weld condition (alloy-*P*-*v*) was performed at least in triplicate to ensure accuracy of the results. Thus, the depth-width pairs of data reported here are the mean of at least three values.

Results and Discussion

Influence of Laser Power and Processing Rate on Weld Morphology

Metallographic images at 30× of cross sections of some butt joints in aluminum alloys have been included in Fig. 2. As can be easily observed, the morphology of the welds follows a semicircle shape, with a depth/width ratio of up to 0.5, confirming that the laser welding was performed under a conduction regime.

The so-called "welding percentage" parameter was measured macroscopically in each weld. This parameter depicts the ratio between the length of the welded interface and the length of the interface exposed to the laser beam (Ref. 1). Thus, the welding percentage can range between 0%, when no joint is achieved, and 100%, when the specimens are totally welded. The welding percentage measurements are shown in Fig. 3. Generally, in the six studied alloys, the welding percentage decreases as the input energy diminishes (lower *P* and higher *v*). However, very high energies can also lead to a decrease of this parameter, as can be observed in the AA2024 welds obtained at 5 mm·s^{-1}. These results show that *P* and *v* conditions should be carefully optimized for each alloy to obtain appropriate welds. Note that the 5083 alloy could be welded at higher welding speeds than the others, although with low welding percentage values — Fig. 3. According to the obtained results, it can be stated that the six aluminum alloys can be generally welded with values of *P* between 1.5 and 2.75 kV and *v* between 5 and 25 mm·s^{-1}. Under these conditions, the welding percentages are usually higher than 50%.

The width *(w)* and depth *(d)* values of all welds obtained under the conditions indicated in Table 2 have been included in Table 3. From the overall data obtained, it can be emphasised that high penetration welds could be achieved under the conduction regime for the six aluminum alloys. Complete penetration was reached in four alloys, 1050 (2 mm), 2024 (2 mm), 5083 (3 mm) and 7075 (2 mm). The higher thickness of the other two alloys, 2017 and 6082 (4 mm), makes complete-joint-penetration welding more difficult to achieve under the conduction regime. A comparison of welds generated on samples with the same thickness is carried out in the next section.

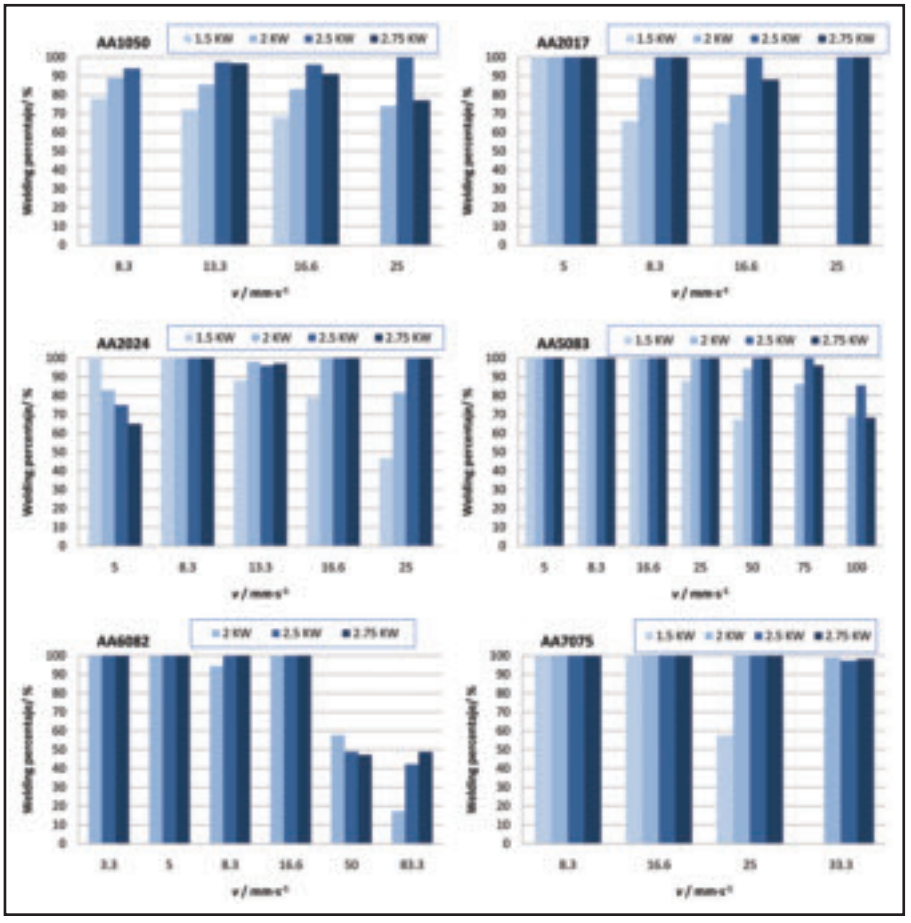

Fig. 3 — Welding percentage of aluminum alloys as function of the welding speed (v) *and the laser power* (P).

Subsequently, the measured *w* and *d* values were fitted to Equation 1, allowing the estimation of *a* and *b*, constants for each alloy. The results are shown in Table 4. The experimental conditions leading to complete penetration (high energy) were not taken into account to the data fitting of Equation 1, as in these cases, the *d*/*w* relationship deviates from its normal tendency. Neither the low energetic conditions giving to welding percentage values lower than 60% were considered to the fitting. Our studies have shown that *d*/w values are practically independent of *P*, being mostly modulated by *v*. Thus, taking into account the experimental relationship between the *d*/*w* values and *v* (Equation 2), *a*' and *b*' constants were estimated. The obtained *a*' and *b*' values are included in Table 5. Finally, *d* values (in mm) were estimated taking into account the experimental variables (*P* and *v*) and the calculated fitting constants (*a*, *b*, *a*', and *b*'), as indicated in Equation 3. Taking into account that the fittings provide positive *a* values and negative *b* values in all cases, it can be deducted that the lower are the absolute values of both coefficients, the deeper are the welds obtained. Similarly, *a*' and *b*' are related to the weld shape, the dependency of the *d*/*w* ratio on the welding speed (*v*) being modulated by *b*'. Thus, the higher are *a*' and *b*' for an alloy, the narrower will be the welds generated.

$$\frac{P}{v \cdot d} = a + \frac{b}{w} \quad (1)$$

$$d / w = a' + \frac{b'}{v} \quad (2)$$

$$d = \frac{P - b \cdot b'}{a \cdot v} - \frac{b \cdot a'}{a} \quad (3)$$

The obtained penetration values of welds obtained for the six aluminum alloys under different *P* and *v* have been compared with those values estimated from Equation 3. These data have been jointly plotted in Figs. 4–9. It can be confirmed that, keeping invariable the experimental conditions, the estimated values are very similar to the experimental ones, proving the validity of the proposed analytical expression.

Weldability Order of Aluminum Alloys

From the obtained results in the previ-

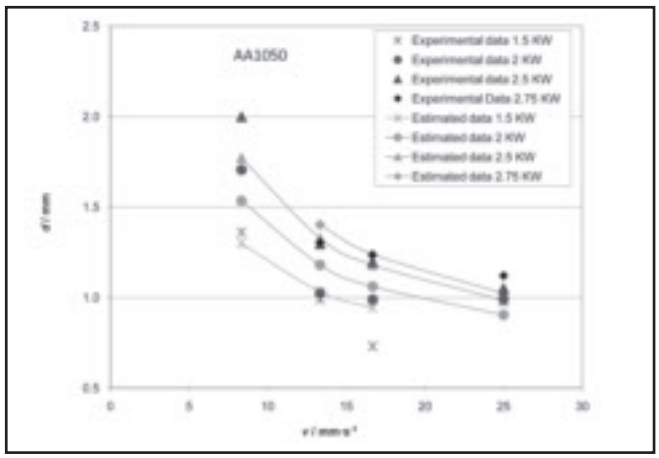

Fig. 4 — Measured and estimated penetration values (d) *of 1050 butt joints, in function of the processing rate* (v) *and the laser power* (P).

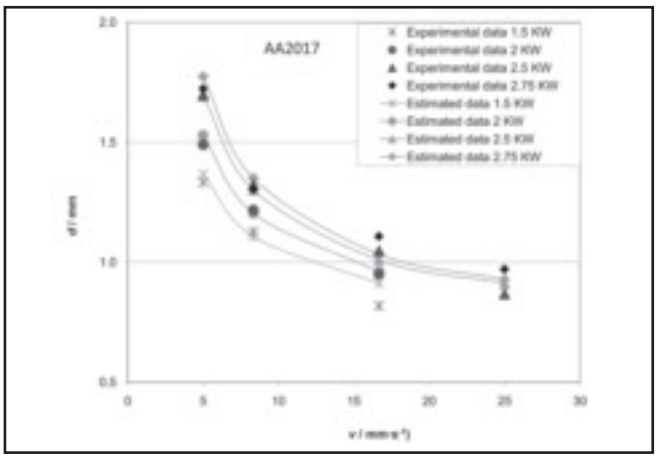

Fig. 5 — Measured and estimated penetration values (d) *of 2017 butt joints, in function of the processing rate* (v) *and the laser power* (P).

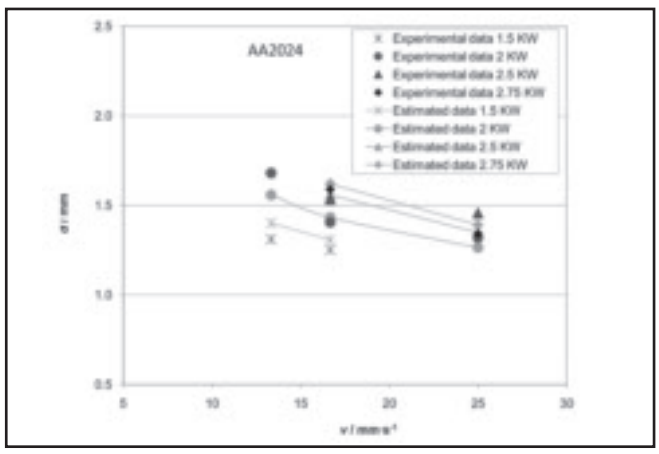

Fig. 6 — Measured and estimated penetration values (d) *of 2024 butt joints, in function of the processing rate* (v) *and the laser power* (P).

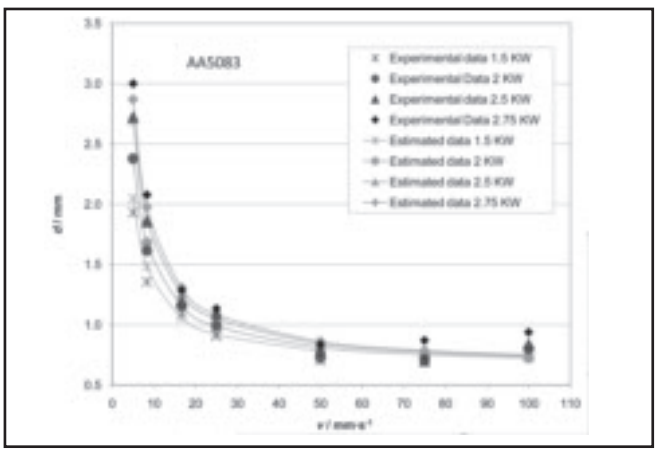

Fig. 7 — Measured and estimated penetration values (d) *of 5083 butt joints, in function of the processing rate* (v) *and the laser power* (P).

ous section, it can be easily appreciated that under the same experimental conditions (*P* and *v*), the weld depth values are different for each alloy studied. As the thickness of the samples is important in the conduction regime, in order to compare the weldability of the six alloys, different bead-on-plate welds were generated on samples with the same thickness (2 mm). The penetration *(d)*, *d*/*w* ratio, and the volume of fused material (V_F) were the parameters measured to characterize the welds. It has been considered that the higher the values of *d* and V_F for a certain alloy, the higher its (laser) weldability. Table 6 summarizes the obtained results. It is clear that 5083 is the alloy with the highest weldability (highest *d* and V_F values), followed by 7075. Thirdly, 2017, 2024, and 6083 show a lower weldability than 5083 and 7075; these three alloys presenting comparable values of the analyzed parameters. Lastly, 1050 is the alloy presenting the lowest weldability, showing the welds with lowest values of *d* and V_F. This weldability order of aluminum alloys is in good agreement with earlier results obtained by Martukanitz et al. (Refs. 21–23), in which CO_2 and Nd:YAG lasers were employed to weld different aluminum alloys under the keyhole regime.

Weld cracking of aluminum alloys has to be taken into account in LBW because of their relatively high thermal expansion, large change in volume upon solidification, and wide solidification temperature range (Ref. 22). The susceptibility to cracking solidification was seen to be different for the studied aluminum alloys: 5083 is the alloy presenting the lowest cracking susceptibility, followed by 7075. Aluminum Alloys

Table 4 — *a'* and *b'* Values Estimated from Equation 1

Alloy	*a* (kJ·mm^{-2})	*b* (kJ·mm^{-1})	R^2
1050	0.2535	-0.391	0.3767
2017	0.6106	-1.4377	0.9312
2024	0.238	-0.4944	0.7641
5083	0.3043	-0.647	0.9694
6082	0.4900	-0.716	0.9002
7075	0.1547	-0.2889	0.7792

Table 5 — *a'* and *b'* Values Estimated from Equation 2

Alloy	*a'*	*b'* (mm·sec^{-1})	R^2
1050	0.3133	0.8910	0.5464
2017	0.3010	0.3398	0.7578
2024	0.4413	0.0947	0.0044
5083	0.3030	0.9636	0.8910
6082	0.2934	0.5123	0.9218
7075	0.3131	2.2323	0.7986

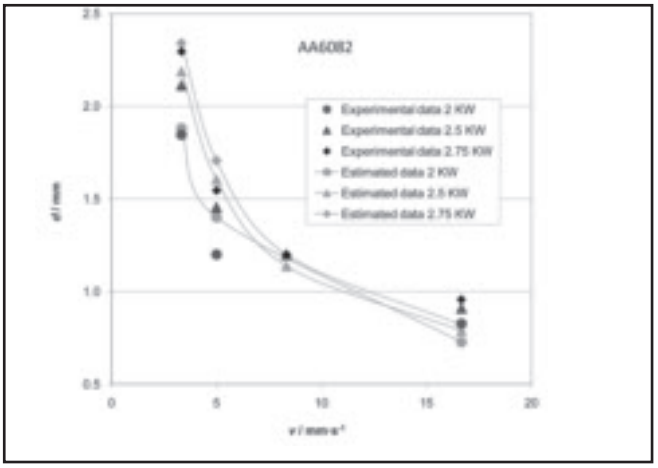

Fig. 8 — Measured and estimated penetration values (d) *of 6082 butt joints, in function of the processing rate* (v) *and the laser power* (P).

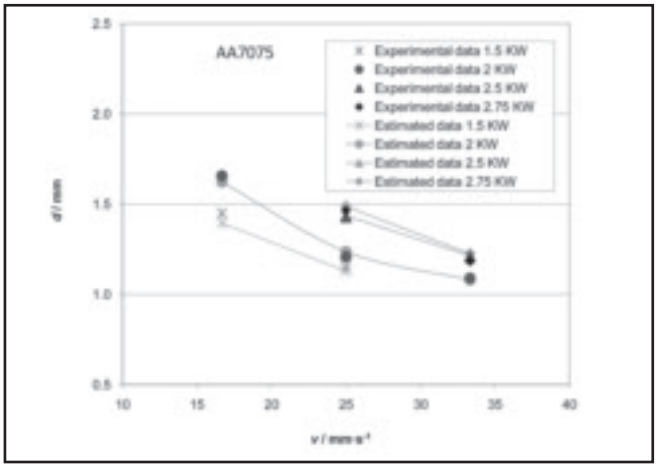

Fig. 9 — Measured and estimated penetration values (d) *of 7075 butt joints, in function of the processing rate* (v) *and the laser power* (P).

2017, 2024, 6082, and 1050 presented higher cracking susceptibility, their weld beads showing similar levels of solidification cracks. This different susceptibility to solidification cracking can also be quantified taking into account the lower limit of the laser fluence above which welds free of cracks are generated for each alloy. It has been experimentally observed that under low fluence LBW treatments, the low-penetration welds generated suffered from cracking, the low energy applied not being able to stabilize the weld pool and generate the joint. Interestingly, the lower limit of the laser fluence above which the welds (without cracks) become stable was different for each alloy, basically depending on the different susceptibility to the solidification cracking of the alloys. According to Table 3, the minimum laser fluence to obtain welds with welding percentages higher than 80% is 5.5 kJ·cm^{-2} for AA1050 (2 kW and 16 mm/s), 5.5 kJ·cm^{-2} for AA2017 (2 kW and 16 mm/s), 5.5 kJ·cm^{-2} for AA2024 (2 kW and 16 mm/s), 1.1 kJ·cm^{-2} for AA5083 (2.5 kW and 100 mm/s), 5.5 kJ·cm^{-2} for AA6082 (2 kW and 16 mm/s), and 2.7 kJ·cm^{-2} for AA7075 (2 kW and 33 mm/s). These minimum laser fluence values are observed to reveal the relative susceptibility to solidification cracking of the different alloys (from lowest to highest susceptibility: 5083 > 7075 > 2017 = 2024 = 6082 = 1050). These results are in good agreement with the obtained data regarding the weld penetration ability, allowing the authors to establish the following weldability order: 5083 > 7075 > 2017 = 2024 = 6082 > 1050.

The data included in Tables 1 and 6 allow the authors to analyze the relative influence of alloying elements on the weldability of aluminum alloys under the conduction regime. Thus, according to these results, the magnesium content is seen to be the most influencing element, being the main compositional factor controlling the different bead weld penetration of aluminum alloys. Thus, the alloy with highest content of this element (5083) is the one with highest weldability. The following alloy in weldability is the 7075, the one presenting the second-highest magnesium content. These arguments agree with those reported in the recent literature, in which the magnesium content is also indicated to improve the laser weldability, as it stabilizes the weld pool and improves the absorption of laser energy (Refs. 1, 5). This element is also claimed to decrease the thermal diffusivity and conductivity of the aluminum alloys limiting the heat conduction, and consequently, allowing the concentration of energy in the weld pool (Refs. 5, 24, 25). In this context, the thermal conductivity has been previously reported (Refs. 2, 26–28) to be a key physical property affecting the weldability of aluminum alloys under the conduction regime, providing their relatively high values in comparison with other alloys. It is also indicated in Ref. 5 that Mg in 5XXX series alloys increases the bead penetration under keyhole welding, as a consequence of the keyhole stabilization and the decrease of the threshold power density, as a consequence of their high vapor pressures. It is, therefore, clear that magnesium is a very active element, decreasing the surface tension of the molten metal and enhancing the melting efficiency (Ref. 5).

Other volatile elements, such as zinc in 7XXX series alloys, have been claimed in the literature to increase the bead penetration in laser welding (Ref. 29). Thus, this alloying element is indicated to improve the weldability of aluminum alloys under keyhole regime (Ref. 25). Zinc content generally decreases both the thermal conductivity and the melting temperature of aluminum. The results obtained in the present work (Tables 1 and 6) indicate that the weldability of aluminum alloys is less influenced by this alloying element than by magnesium. Thus, although Alloy 7075 has higher volatile compounds (7.79% of Mg + Zn content) than Alloy 5083 (4.22% of Mg + Zn content), it is Alloy 5083 that has better weldability. This fact suggests that the relatively high weldability of 7075 may be mainly attributed to the 2.32% Mg, although the 5.47% of Zn can also contribute at a lower extent.

The addition of silicon to aluminum is also known to improve its weldability (Ref. 25), as it decreases the thermal conductivity, decreases the melting temperature, and improves the fluidity (Ref. 30). The Si content is also claimed to decrease the thermal conductivity of Al-Si diamond composites and Al-Si matrix (Ref. 31). From the results obtained in the present work, it is difficult to state clear conclusions regarding the effect of silicon on the weldability of aluminum alloys. Even though taking into account the composition of the alloys with similar weldability (2017, 2024, and 6082) in

Table 6 — Depth/Width (*d*/*w*) and Fused Volume (V_F) of Bead-on-Plate Welds Performed at Two Processing Rates on the Six Aluminum Alloys

	v (mm/s) 16.6		*v* (mm/s) 33.3	
Alloy	d/w (mm/mm)	V_F (mm^3)	d/w (mm/mm)	V_F (mm^3)
1050	1.10/2.61	135	0.52/2.00	49
2017	1.48/3.32	231	0.82/2.42	93
2024	1.45/3.07	210	0.96/2.62	118
5083	> 2/4.01	379	1.16/2.87	157
6082	1.48/3.14	219	0.79/2.42	90
7075	> 2/3.84	340	0.96/2.70	122

Table 1, it is possible to establish that silicon content moderately contributes to enhancing the weld penetration. Thus, 6082 and 2017 alloys have lower magnesium content and higher silicon content than 2024. Providing that Alloys 6082, 2017, and 2024 present similar weldability, it is deducted that the lower magnesium content is compensated with the higher silicon content. However, similar to the influence of the Zn content, Si seems to have a much lower effect than magnesium on the weldability of aluminum alloys.

To sum up, the weldability order observed in the six aluminum alloys has been as follows: 5083 > 7075 > 2017 = 2024 = 6082 > 1050. The magnesium has been seen to be the most influencing alloying element on improving the weldability of aluminum alloys. Zinc and silicon are also seen to improve the weldability, although the influence of these latter alloying elements seems to be lower than magnesium. These elements are generally reported to decrease the thermal conductivity and the melting temperature, both effects being beneficial for increasing the weldability.

Conclusions

In this work, six aluminum alloys (1050, 2017, 2024, 5083, 6082, and 7075) were welded under the conduction regime using a high-power laser diode. High-penetration butt joints could be achieved in each alloy when optimizing the experimental conditions. In fact, welds of the six alloys with higher penetration than those previously reported under the conduction regime have been obtained.

The depths and widths of the obtained welds were fitted to a simple mathematical equation proposed by the authors. The expression allowed the estimation of the weld depth for each alloy under different laser welding conditions, taking into account only the input values of laser power and welding speed, providing a reasonable fitting to the measured experimental penetration values.

Finally, the weldability of the six aluminum alloys were compared, taking into account the depth, shape, and fused volume measured on bead-on-plate welds. The weldability order, taking into account both the weld penetration ability and the susceptibility to solidification cracking, was seen to be 5083 > 7075 > 2017 = 2024 = 6082 > 1050. The magnesium content is observed to be the most influencing alloying element on the weldability of aluminum alloys. Zinc and silicon are also seen to improve the weldability, although at a lower extent than magnesium. These elements decrease the thermal conductivity and the melting temperature, increasing, therefore, the weldability of aluminum alloys.

Acknowledgments

The present work has been financially supported by the Ministerio de Educación y Ciencia (project DELATIAL, Reference MAT2008-06882-C04-02 and project LENTEC, Ref. PTQ-09-01-00629) and by the Junta de Andalucía (project SOLDATIA, Ref. TEP-6180). The authors would like to thank students Xavier Bouchon and Maëlys Le Coz, from "École polytechnique de l'université de Nantes" for their active collaboration on these projects.

References

1. Sánchez-Amaya, J. M., Delgado, T., González-Rovira, L., and Botana, F. J. 2009. Laser welding of aluminum alloys 5083 and 6082 under conduction regime. *Appl. Surf. Sci.* 255(23): 9512–9521.

2. Sánchez-Amaya, J. M., Delgado, T., De Damborenea, J. J., López, V., and Botana, F. J. 2009. Laser welding of AA 5083 samples by high power diode laser. *Sci. Technol. Weld. Join.* 14 (1): 78–86.

3. Ding, R. G., Ojo, O. A., and Chaturvedi, M. C. 2007. Laser beam weld-metal microstructure in a yttrium modified directionally solidified Ni_3Al-base alloy. *Intermetallics* 15: 1504–1510.

4. Akhter, R., Ivanchev, L., and Burger, H. P. 2007. Effect of pre/post T6 heat treatment on the mechanical properties of laser welded SSM cast A356 aluminum alloy. *Mat. Sci. Eng. A–Struct.* 447: 192–196.

5. Kuo, T. Y., and Lin, H. C. 2006. Effects of pulse level of Nd-YAG laser on tensile properties and formability of laser weldments in automotive aluminum alloys. *Mat. Sci. Eng. A–Struct.* 416: 281–289.

6. Yan, J., Zeng, X., Gao, M., Lai, J., and Lin, T. 2009. Effect of welding wires on microstructure and mechanical properties of 2A12 aluminum alloy in CO_2 laser-MIG hybrid welding. *Appl. Surf. Sci*. 255 (16): 7307–7313.

7. Campana, G., Ascari, A., Fortunato, A., and Tani, G. 2009. Hybrid laser-MIG welding of aluminum alloys: The influence of shielding gases. *Appl. Surf. Sci.* 255(10): 5588–5590.

8. Tobar, M. J., Lamas, I. M., Yáñez, A., Sánchez-Amaya, J. M., Boukha, Z., and Botana, F. J. 2010. Experimental and simulation studies on laser conduction welding of AA5083 aluminum alloys. *Physics procedia* 5: 299–308.

9. Duley, W. W. 1998. *Laser Welding*, Chapter 3 and 4. New York, N.Y.: John Wiley & Sons.

10. Okon, P., Dearden, G., Watkins, K., Sharp, M., and French, P. 2002. *Proc. 21st Int. Cong. on Applications of Lasers and Electro-Optics (ICALEO 2002)*. Scottsdale, Ariz., October 2002, Laser Institute of America, pp. 233–241.

11. Zhao, H., and DebRoy, T. 2001. Weld metal composition change during conduction mode laser welding of aluminum Alloy 5182. *Metall. Mater. Trans. B* 32B: 163–172.

12. Shi, Y., Zhonga, F., Li, X., Gong, S., and Chen, L. 2007. Effect of laser beam welding on tear toughness of a 1420 aluminum alloy thin sheet. *Mat. Sci. Eng. A–Struct.* 465: 153–159.

13. Bassani, P., Capello, E., Colombo, D., Previtali, B., and Vedani, M. 2007. Effect of process parameters on bead properties of A359/SiC MMCs welded by laser. *Compos. Part A-Appl. S.* 38: 1089–1098.

14. Spina, R., Tricarico, L., Basile, G., and Sibillano, T. 2007. Thermo-mechanical modeling of laser welding of AA5083 sheets. *J. Mater. Process. Tech.* 191: 215–219.

15. Ancona, A., Sibillano, T., Tricarico, L., Spina, R., Lugara, P. M., Basile, G., and Schiavone, S. 2005. Comparison of two different nozzles for laser beam welding of AA5083 aluminum alloy. *J. Mater. Process. Tech.* 164–165: 971–977.

16. Sibillano, T., Ancona, A., Berardia, V., Schingaro, E., Basilea, G., and Lugara, P. M. 2006. A study of the shielding gas influence on the laser beam welding of AA5083 aluminum alloys by in-process spectroscopic investigation. *Opt. Lasers Eng.* 44: 1039–1051.

17. Tricarico, L., Spina, R., Sorgente, D., Ancona, A., Sibillano, T., and Basile, G. 2007. Experimental analysis of AA5083 butt joints welded by CO_2 laser. *Key Eng. Mat.* 344: 745–750.

18. Haboudou, A., Peyre, P., Vannes, A. B., and Peix, G. 2003. Reduction of porosity content generated during Nd:YAG laser welding of A356 and AA5083 aluminum alloys. *Mat. Sci. Eng. A–Struct.* 363: 40–52.

19. Abe, N., Tsukamoto, M., Maeda, K., Namba, K., and Morimoto, J. 2006. Aluminum alloy welding by using a high power direct diode laser. *J. Laser Appl.* 18(4): 289–293.

20. Howard, K., Lawson, S., and Zhou, Y. 2006. Welding aluminum sheet using a high-power diode laser. *Welding Journal* 85(5): 101–110.

21. Martukanitz, R. P., Jan, R., Armao, F. G., Pickering, E. R., and Baldantoni, A. 1994. Laser beam welding of aluminum alloys for automotive applications. *Proceedings of the Society of Automotive Engineers International Congress and Exposition*, Society of Automotive Engineers, SAE Technical Document 940158.

22. Martukanitz, R. P., and Smith, D. J. 1995. Development of the laser beam welding process for aluminum alloys. *Proceedings of the 6th International Conference on Aluminum Weldments*. American Welding Society, pp. 309–323.

23. Martukanitz, R. P., Altshuller, B., Armao, F. G., and Pickering, E. R. 1996. Properties and characteristics of laser beam welds of automotive alloys. *Proceedings of the Society of Automotive Engineers International Congress and Exposition*, Society of Automotive Engineers, SAE Technical Document 960168.

24. Van Horn, K. R. 1978. *Aluminum*. Metals Park, N.Y.: ASM, pp. 167–177.

25. Sakamoto, H., Shibata, K., and Dausinger, F. 2003. Effect of alloying elements on weld properties in CO_2 laser welding of aluminum alloys. *Welding Journal* 82(7): 509–513.

26. Luijendijk, T. 2000. Welding of dissimilar aluminum alloys. *J. Mater. Process. Tech.* 103: 29–35.

27. Chen, B. K., Thomson, P. F., and Choi, S. K. 1992. Computer modelling of microstructure during hot flat rolling of aluminum. *Mater. Sci. Tech.* 8: 72–77.

28. Ahmed, H., Wells, M. A., Maijer, D. M., Howes, B. J., and van der Winden, M. R. 2005. Modelling of microstructure evolution during hot rolling of AA5083 using an internal state variable approach integrated into an FE model. *Mat. Sci. Eng. A–Struct.* 390(1-2): 278–290.

29. Zhao, H., White, D. R., and DebRoy, T. 1999. Current issues and problems in laser welding of automotive aluminum alloys. *Int. Mater. Rev.* 44(6): 238–266.

30. *www.esabna.com/us/en/education/knowledge/qa/*. How and why alloying elements are added to aluminum. By T. Anderson, ESAB, 2010.

31. Zhang, Y., Wang, X., and Wu, J. 2009. *International Conference on Electronic Packaging Technology & High Density Packaging (ICEPT-HDP)*, pp. 708–712.